Proceedings of the 5th International Conference on Materials Chemistry and Environmental Engineering
DOI: 10.54254/2755-2721/123/2025.19595

A Novel Layered Perovskite $RbCeNb_2O_6$-xNx as a Nanosheet Photocatalyst for CH_4 Production

Jin Huang[1,a,*]

[1]*Lauralton Hall, 200 High St, Milford, CT, USA*
a. huangjin064@gmail.com
**corresponding author*

Abstract: The production and recovery of methane as a potential clean energy source not only reduces carbon emissions and mitigates climate change, but also improves energy efficiency compared with conventional fossil fuels. In recent years, the study of efficient catalytic conversion of hydrocarbons using inclusion crystals as photocatalysts has been widely reported. This study proposes a new perovskite $RbCeNb_2O_6$-xNx catalysts in the form of nanosheets can be used for photocatalytic methane conversion. Artificially synthesized layered perovskites exhibit excellent reaction properties due to the increased surface-active area. In synthesis, $RbLnNb_2O_7$ (Ln = La, Nd, Pr, Ce) was successfully synthesized by the ceramic solid phase synthesis method, which was based on a powder sample of lamellar-coated crystals. Subsequent nitrogen addition resulted in the synthesis of $RbLaNb_2O_6$-xNx, $RbNdNb_2O_6$-xNx, $RbPrNb_2O_6$-xNx and $RbCeNb_2O_6$-xNx catalysts in the form of nanosheets. All four synthesized catalysts were nitrogen-modified during processing, and the synergistic effect between oxygen and nitrogen (ratio=16.94) was applied to perovskite nanosheets through defect engineering. The methane catalytic properties were compared, and the material structures were characterized by atomic force microscopy, transmission electron microscopy, X-ray diffraction and XPS. The results show that $RbCeNb_2O_6$-xNx can produce the most methane, 70% more methane under the same conditions, compared with the other three, and had the best catalytic effect.

Keywords: defect engineering, layered perovskites, photocatalysts of methane production, $RbCeNb_2O_6$-xNx perovskite nanosheet.

1. Introduction

With the gradual increase in global population, serious problems such as ecological damage, environmental pollution and resource scarcity are becoming increasingly serious worldwide. These problems are particularly serious in developing countries and could lead to an unprecedented crisis [1]. CH_4 can be used as a local source of clean energy, which accounts for about one-third of the current global warming from anthropogenic greenhouse gases, and as a substitute for carbon dioxide [2]. For the sake of the environment, we can try to improve the photocatalytic performance by synthesizing some new chemical photocatalysts to improve the photocatalytic performance, and then validate some of the substances by means of chemical techniques through characterization and other steps, and convert or generate important fuels and chemicals, such as CH_4, in order to reduce the dependence of human beings on fossil energy sources, and thus improve the environment. In this

© 2025 The Authors. This is an open access article distributed under the terms of the Creative Commons Attribution License 4.0 (https://creativecommons.org/licenses/by/4.0/).

DOI: 10.54254/2755-2721/123/2025.19595

study, $RbLaNb_2O_7$ (Ln=La, Nd, Pr, Ce) will be used as a reference to obtain its powder samples; the synthesis of nanosheets carried out in this study is expected to lead to progress in the field of photocatalysts, since high crystallinity and large surface area are the key to achieve efficient photocatalysts and nanosheets satisfy these two requirements. Although photocatalysis has realized applications in the field of environment with a certain scale, it still needs to break through in the direction of energy.

2. Methodology

To synthesize bulk powder samples of perovskite nanosheets $RbLnNb_2O_7$ (Ln=La, Nd, Pr, Ce), the ceramic solid-phase synthesis method developed by Michael Hayward et.al. [3] was used. The nitrogen addition step was then carried out so that a comparison of the catalytic effects could be made. First, precursors of Nd_2O_3, La_2O_3, Pr_2O_3, Nb_2O_5 and CeO_2 were dried at 1173 K before use. The lanthanide metal oxides were ground with a molar excess of 50% Rb_2CO_3 and the mixture was heated at 1223 K for 12 hours before grinding. The prepared powder (≈0.3 g at a time) was heated at 1223 K for 24 hours at a rate of 10 K/min at a flow rate of 500 ml/min NH3 and then cooled naturally to room temperature. Catalysts prepared by the above process will continue to be characterized by nitriding. The prepared $RbLnNb_2O_7$ (Ln = lanthanum (La), neodymium (Nd), praseodymium (Pr), cerium (Ce)) sample powders (≈0.3 g at a time) were then heated at 1223 K for 24 hours at 10 K/min under a flow rate of 500 ml/min of NH3 and then cooled to room temperature. Nitrogen was added to four samples, and XRD [5], TEM [6], and SEM [7], XPS [8] were used to select the most effective catalyst, and GC [9] was used to verify the effect of CH_4 production.

3. Results and discussions

3.1. Characterization of crystal structure

The perovskite family of $RbLnNb_2O_7$ is involving double-/triple-layered Dion-Jacobson and Riddlesden-Popper members, tetragonal structure. The XRD analysis in Figure 1. compares the XRD spectra before and after nitrogen addition. The data in the XRD of the synthesized catalysts conformed to the standard card of $RbLnNb_2O_7$, respectively, and were analyzed at 2θ = 8.027°, 24.437°, 28.233°, 32.819°, 33.691°, 37.055°, 40.229°, 4.871°, 47.113°, 53.448°, 55.807°, 58.392°, 59.137°, 64.15°5 and 68.805°, the diffraction peaks appeared, which were due to the X-ray diffraction caused by the interatomic distance in the crystal structure. And the angle of the diffraction peaks shifted with different Ln, which is due to the substitution of a part of calcium sites (Ca-sites) in the crystal structure of $RbLnNb_2O_7$, by different rare earth elements (La, Nd, Pr, Ce). Compared to $RbLnNb_2O_7$, $RbLaNb_2O_6$-xNx has a distinct amorphous peak indicating that the final product is not a fully crystalline material. The ionic radius of the rare earth elements differs from that of the calcium ions, so when the rare earth elements replace the calcium sites, the crystal structure is distorted, resulting in a shift in the position of the diffraction peak. For $RbCeNb_2O_6$-xNx, due to the larger ionic radius ofCe ions, their substitution of calcium sites causes lattice distortion. This distortion leads to the entry of nitrogen atoms in the crystal structure into the lattice and the formation of a nitrogen-modified catalyst for $RbCeNb_2O_6$-xNx. Nitrogen modification can increase the number of active sites of the catalyst and enhance the adsorption capacity and reactivity of methane, thus promoting the methane conversion reaction. As a result, the $RbCeNb_2O_6$-xNx catalyst has better catalytic effect and higher methane yield relative to the other three catalysts. This is due to the lattice distortion induced by the substitution ofCe ions for calcium sites as well as the enhanced catalytic activity from nitrogen modification. $RbNdNb_2O_6$-xNx, $RbPrNb_2O_6$-xNx, and $RbCeNb_2O_6$-xNx exhibit similar behavior. As literature review, the “bun peak” represents non-crystallization [10].

DOI: 10.54254/2755-2721/123/2025.19595

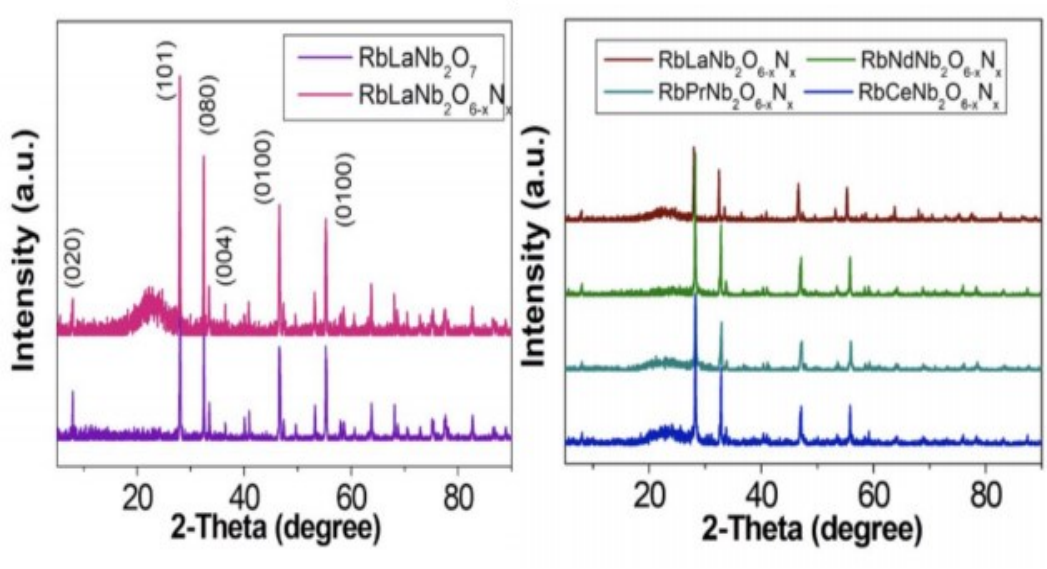

Figure 1: XRD pattern offour catalysts [15]

3.2. Photocatalytic Reaction

The XPS spectra are then combined with their counterparts according to the binding energy cross-reference table, where N1s are clearly present, and the binding energy cross-reference table shows that nitrogen is picked up.

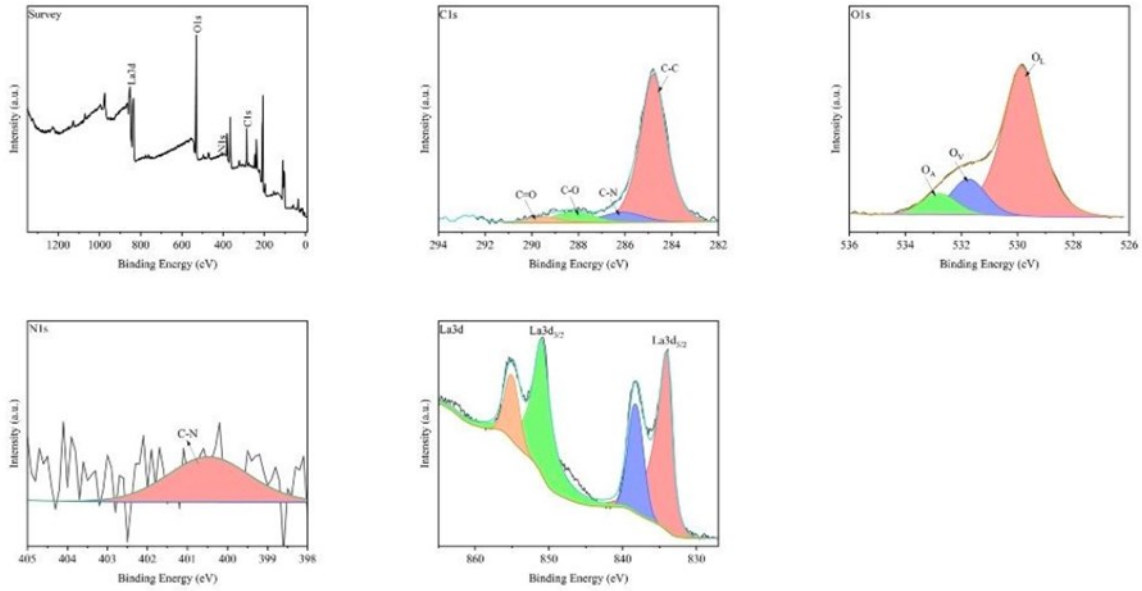

Figure 2: Photocatalytic reaction loaded ≈($RbLaNb_2O_6$-xNx)nanosheets in C 1s; O 1s; N 1s; and Ce3dXPS narrow spectra. [16]

The XPS spectra of the four products are shown in Figures above, and obvious N1s signals were detected in all four samples (orbitals) N belongs to the 3rd order nitrogen, indicating that after nitrogen addition, the nitrogen atoms are connected to the catalyst body molecules in the form of molecular bonds, and the relative N/O ratios are not significant. and the relative N/O ratios are further quantified for each element ($RbLaNb_2O_6$-xNx N/O=0.066; $RbPrNb_2O_6$-xNx N/O=0.085; $RbNdNb_2O_6$-xNx N/O=0.082). $RbCeNb_2O_6$-xNx N/O=0.067), indicating that oxygen atoms are

DOI: 10.54254/2755-2721/123/2025.19595

substituted by nitrogen atoms and the nitrogen substitution occurs overwhelmingly on the surface of the samples, the relative proportion of nitrogen on the surface of the samples is higher [13].

The C1s spectrum of the catalyst in XPS shows several different carbons bonding states, including C-C, C-N, C-O, and C=O. The O1s spectrum, on the other hand, demonstrates several different oxygens bonding states, including OL, OA, and OV. In addition, C-N bonding appears in the N1s spectrum. First, the C-C bonding state in the C1s spectra indicates that the catalyst has a carbon chain structure, which help it to function in organic synthesis reactions. The presence of the C-N bonding state implies that the catalyst has the potential for the conversion of nitrogen-containing compounds. Whereas the presence of C-O and C=O bonding states suggests that the catalyst plays an important role in oxidation reactions. OL in the O1s spectrum indicates metallic oxygen on the catalyst surface, OA represents adsorbed oxygen, and OV indicates defective oxygen on the catalyst surface. These different oxygen bonding states can affect the activity and selectivity of the catalyst.

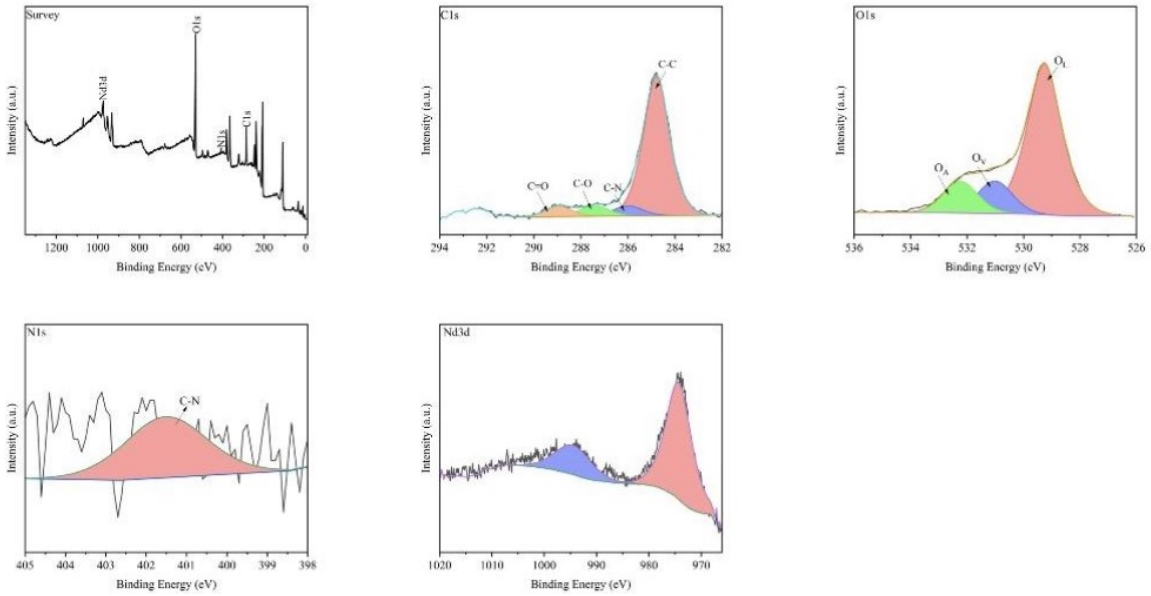

Figure 3: Photocatalytic reaction loaded ≈(RbNdNb2O6-xNx)nanosheets in C 1s; O 1s; N 1s; and Ce3dXPS narrow spectra [17]

The C-N bonding state in the N1s spectrum suggests that the catalyst has catalytic activity for the conversion of nitrogen- containing compounds. This is of potential significance for the application of catalysts in organic synthesis and environmental protection. The presence of La, Nd, Pr and Ce elements in the XPS of $RbLaNb_2O_6$-xNx, $RbNdNb_2O_6$-xNx, $RbPrNb_2O_6$-xNx and $RbCeNb_2O_6$-xNx nanosheet samples, respectively, proved their successful synthesis. Among them, Ce element has good redox ability and can effectively participate in the activation and conversion reaction of methane. In addition, the Nb element in this catalyst also plays an important role in promoting the reaction.

The structure of this composite material has a large specific surface area and abundant active sites, providing more reaction opportunities and adsorption capacity, thus enhancing the efficiency of methane conversion. Secondly, nitrogen modification plays a key role in the improvement of catalyst performance. Through the introduction of nitrogen atoms, the surface properties of the catalysts were modulated, and the number and strength of surface acidic and basic sites were increased. These modified surface sites were able to adsorb and activate methane molecules more efficiently, facilitating the reaction of their conversion into other useful compounds. In addition, nitrogen modification can improve the stability and anti-poisoning properties of the catalyst and extend its service life [13].

DOI: 10.54254/2755-2721/123/2025.19595

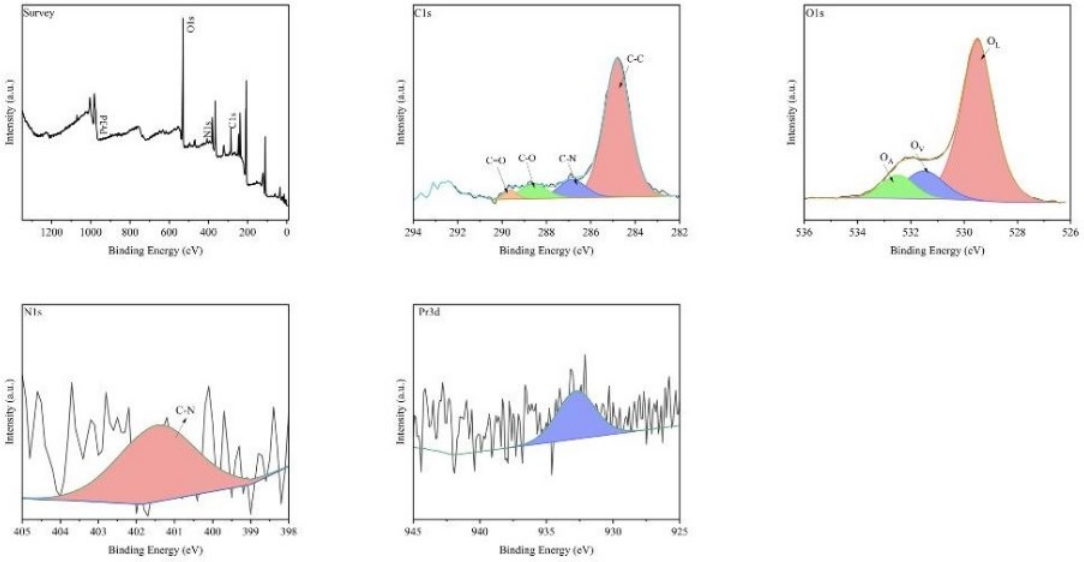

Figure 4: Photocatalytic reaction loaded ≈ ($RbPrNb_2O_6$-xNx)nanosheets in C 1s; O 1s; N 1s; and Ce3dXPS narrow spectra [18]

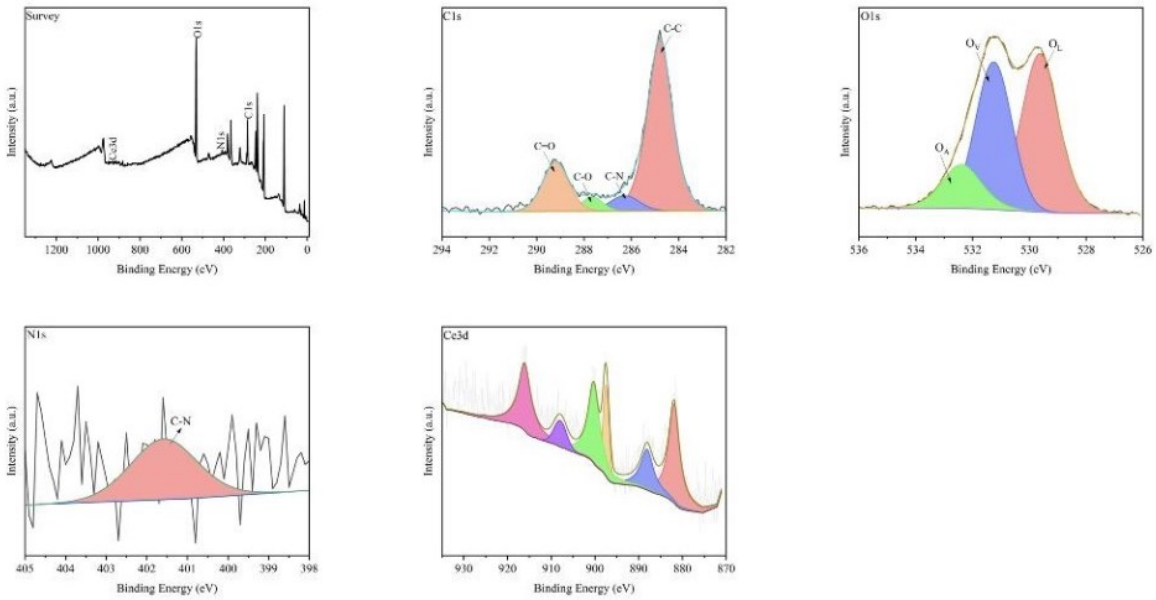

Figure 5: Photocatalytic reaction loaded ≈ ($RbCeNb_2O_6$-xNx)nanosheets in C1s; O1s; N1s; and Ce3d XPS narrow spectra [19]

Table 1: Nitrogen to Oxygen mass ratio offour catalysts

	RbLaNb2O6-xNx	RbNdNb2O6-xNx	RbPrNb2O6-xNx	RbCeNb2O6-xNx
The mass Amount of N (%)	3.66	4.88	5.23	3.79
The mass Amount of O(%)	55.33	57.61	63.71	56.75

DOI: 10.54254/2755-2721/123/2025.19595

For the N/O ratios of the peak responses of XPS, high the N/O ratios indicate the presence of nitrogen compounds, which can act as active sites or cofactors in catalytic reactions, and catalysts with high the N/O ratios are more catalytically active [4]. In other words, high relative abundance usually indicates the presence of nitrogen compounds or oxides that have a positive effect on certain catalytic reactions.

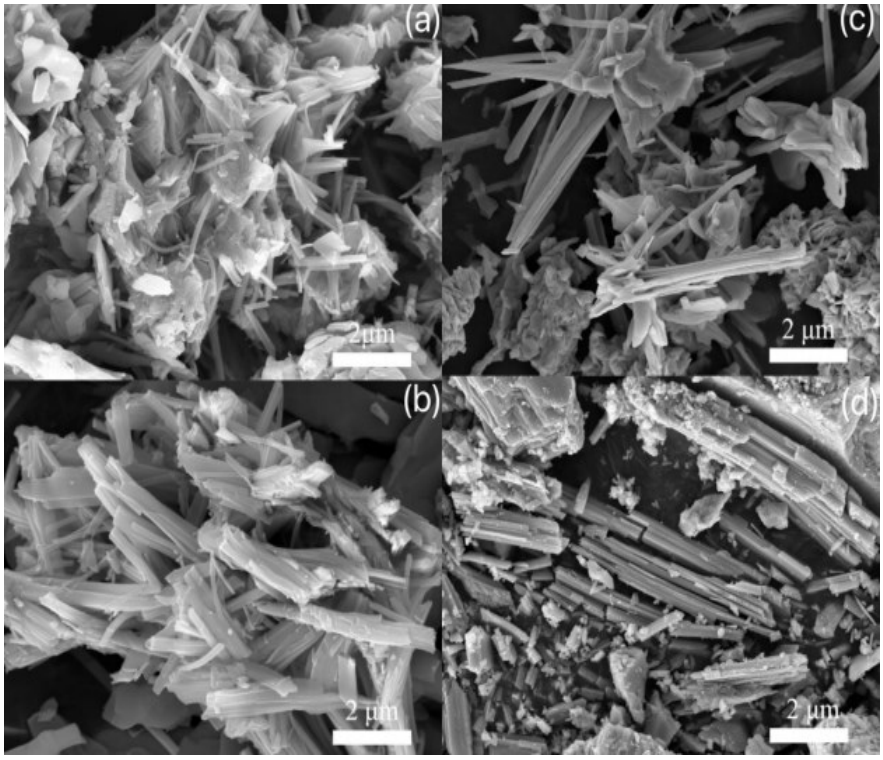

Figure 6: The SEM images of the four catalysts (a= $RbLaNb_2O_6$-xNx; b= $RbPrNb_2O_6$-xNx; c= $RbNdNb_2O_6$-xNx; $RbCeNb_2O_6$-xNx [20]

Observe the nanosheet structure in the SEM image. We can see that the nanosheets are characterized by tiny microcrystals. These tiny microcrystals are due to crystal growth and deformation during the preparation process of ceramic solid phase synthesis method. The presence of tiny microcrystals leads to an increase in the active surface area of the catalyst, which improves the reactivity. During the nitrogen modification process, the crystal structure of the catalyst undergoes some changes. The presence of such microcrystals provides more reactive active sites, thus facilitating the methane-catalyzed reaction. The in-plane crystal orientation is aligned. This means that the crystal structure of the catalyst forms a more ordered crystal structure. This ordered crystal structure provides more stable catalytic activity and contribute to higher methane yield. Large-area single-crystal nanosheets with more dispersed flakes can be observed in the SEM of the $RbCeNb_2O_7$-xNx samples, which suggests that the crystal structure of the catalyst has been highly ordered and the crystal size is larger. This large-area single-crystal nanosheet has provided more active sites and better reaction diffusion properties [12], resulting in higher methane yield and better catalytic effect.

At the end of the reaction, the presence of methane (CH_4) was detected in the gas samples corresponding to all four catalysts, and the intrinsic gases were and are only pure methane, so only one methane component out of the peaks is shown in the peaks graph of the GC. Among them, $RbCeNb_2O_6$-xNx produced the most methane, which was approximately higher than the other two catalysts under the same conditions. The results were calculated by area integration [14].

DOI: 10.54254/2755-2721/123/2025.19595

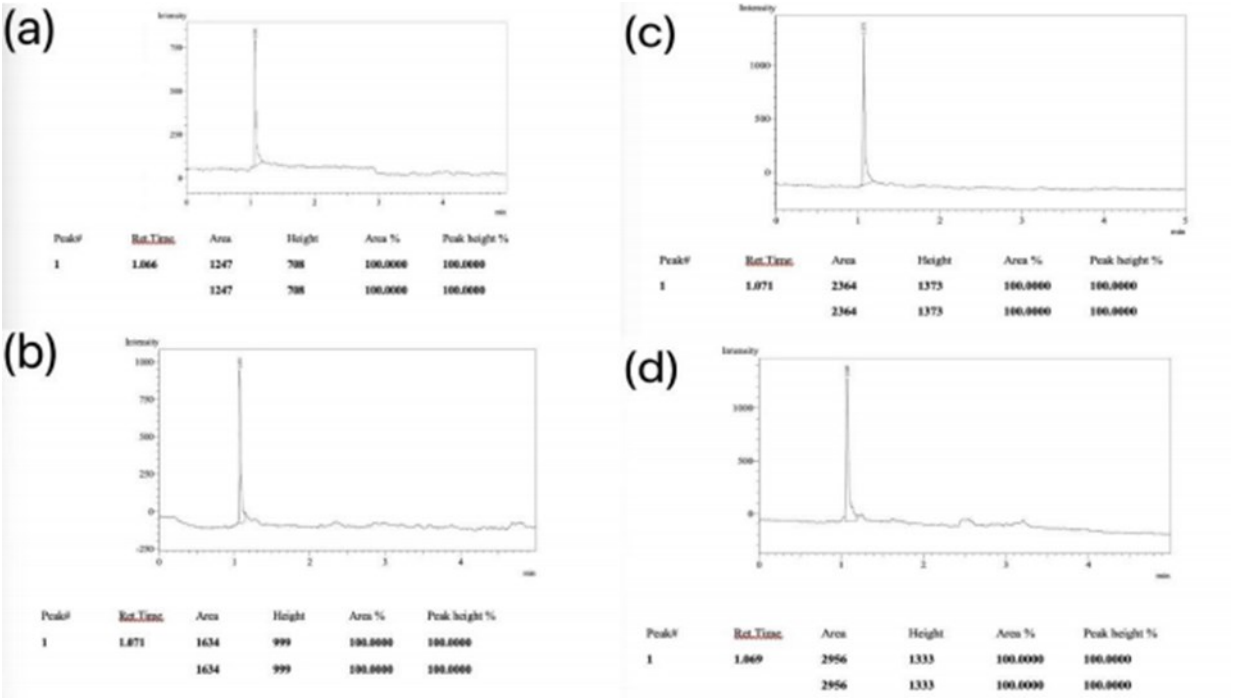

Figure 7: Gas Chromatography of Four Catalysts [21]

Upon comparison, the area of integration for the fourth catalyst is close to 2900+, while the first two catalysts both have an area of integration of 1700+. Using these two numbers, we divide 2900 by 1700 which equals approximately 1.7, so $RbCeNb_2O_6$-xNx is 70% more than the other three catalysts. A series of nanoalloy catalysts were successfully prepared by synthesizing layered tremolite and tremolite nanosheets, and characterization tests were performed to determine the optimal response of the Ce series catalysts. Then the RbCeNb2O6-xNx photocatalyst was synthesized by adding nitrogen. This study showed that the yield and selectivity of $RbCeNb_2O_6$-xNx for CH_4 were improved under the same reaction conditions.

The crystal structures shown in the TEM images have grain sizes of approximately 5-20 nm. Since the gas chromatography experiments measured the best catalyst in the Ce series, the TEM technique was utilized to verify the reason for this. The figure above shows a TEM planar image of $RbCeNb_2O_7$ nanosheets, which is more of a lamellar structure; lamellar structures can have a large effective surface area, and materials with a large surface area are usually more effective at catalyzing reactions, which makes it easier for the substance to meet the reactants, thus increasing the catalytic efficiency. *Figure 7*. shows a magnified TEM image of the nanosheets, which confirms that the nanosheets have a single-crystal structure, with lattice fringes observed in most of the observed regions. The lattice streaks were obtained from the whole nanosheet. The layered structure gives the metal alloy a large electrochemically active surface area and high atom utilization, which can further catalyze the properties of the material and increase its mass activity [11].

DOI: 10.54254/2755-2721/123/2025.19595

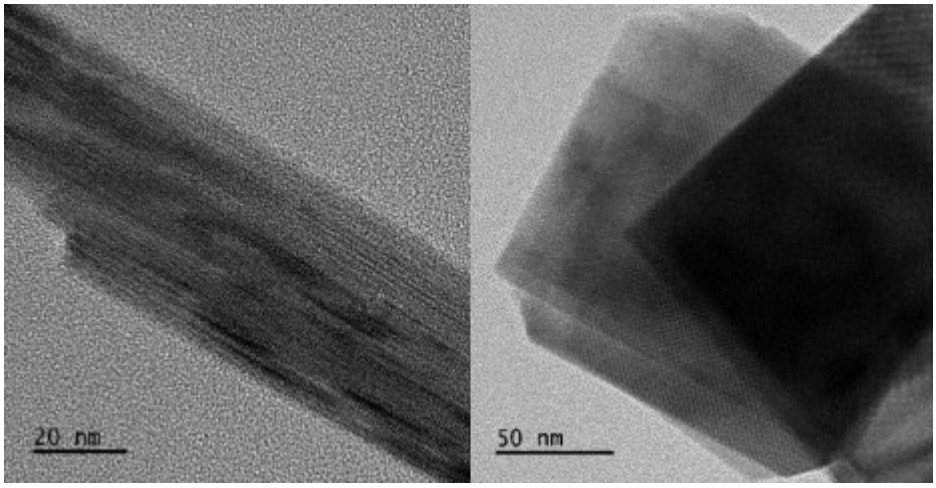

Figure 8: The TEM image ofRbCeNbO6-xNx [22]

In addition, the TEM images show surface defects, and some surface defects (e.g., defect sites, edge sites, etc.) can be used as reaction sites to increase the catalytic effect [11]. These defect sites can provide additional adsorption sites or change the adsorption properties of the reactive substances, thus promoting the catalytic reaction.

Subsequently, we need to characterize the catalytic effect and validate the catalyst using gas-phase photocatalytic reduction of CO_2. After taking 30 mg of the synthesized catalyst powder, the reaction vessel was flushed with carbon dioxide gas, 500 μL of deionized water was added to the reaction vessel and waited for the catalyst to be fully adsorbed for 2 hours. After the catalyst was fully adsorbed, the gas was irradiated for 8 h, and then the gas was inhaled in the reaction vessel with a gas sampling needle, and then detected with a gas chromatograph. After 8 hours of irradiation, the gas was irradiated again. After irradiation for 8 hours, the gas was inhaled in the reaction vessel with a gas sampling needle and then detected by a gas chromatograph. Four samples were compared horizontally using the same conditions.

4. Conclusion

The present study is devoted to the development of a new species of nanoflake-like novel encapsulated crystalline $RbCeNb_2O_6$-xNx catalysts, with the goal of excellent reaction performance by adding nitrogen to increase the surface-active area of the synthesized substances, and finally selecting catalysts with excellent properties that can be used for photocatalytic CH_4 conversion. The four catalysts, $RbLaNb_2O_6$-xNx, $RbNdNb_2O_6$-xNx, $RbPrNb_2O_6$-xNx and $RbCeNb_2O_6$-xNx, were characterized by XRD, XPS, SEM and TEM, and then tested by gas chromatography, which showed that the catalytic effect of the nitrogen addition was superior to that of the catalytic effect of the catalytic effect of the nitrogen addition, and the catalytic effect of the catalytic effect of the catalytic effect of the catalytic effect of the catalytic effect of the catalytic agent was superior to that of the catalytic effect of the nitrogen addition. CH_4; the concentration of CH_4 was different for the four catalysts; based on the surface area of the peaks, the CH_4 productivity of $RbCeNb_2O_6$-xNx was 70% higher than that of the other three catalysts with a thermal conductivity detector.

References

[1] *Piskulova, N. and Gorbanyov, V., 2023. Global Challenges: Environment. In World Economy and International Business: Theories, Trends, and Challenges (pp. 213-233). Cham: Springer International Publishing.*

[2] *Bradford, M.C.J. and Vannice, M.A., 1999. CO2 reforming of CH4. Catalysis Reviews, 41(1), pp.1-42.*

DOI: 10.54254/2755-2721/123/2025.19595

[3] Islam, A., Malek, A., Teo, S.H., Marwani, H.M., Rahman, M.M., Asiri, A.M., Khan, M.A.R., Taufiq-Yap, Y.H. and Awual, M.R., 2023. Smart materials for CO2 conversion into renewable fuels and emission reduction. Sustainable Materials and Technologies, p.e00636.

[4] Kureha, T., Nagase, Y. and Suzuki, D., 2018. High reusability of catalytically active gold nanoparticles immobilized in core–shell hydrogel microspheres. ACS omega, 3(6), pp.6158-6165.

[5] Khan, H., Yerramilli, A.S., D'Oliveira, A., Alford, T.L., Boffito, D.C. and Patience, G.S., 2020. Experimental methods in chemical engineering: X-ray diffraction spectroscopy—XRD. The Canadian journal of chemical engineering, 98(6), pp.1255-1266.

[6] Rao, D.S., Muraleedharan, K. and Humphreys, C.J., 2010. TEM specimen preparation techniques. Microscopy: science, technology, applications and education, 2, p.1232.

[7] Mohammed, A. and Abdullah, A., 2018, November. Scanning electron microscopy (SEM): A review. In Proceedings of the 2018 International Conference on Hydraulics and Pneumatics—HERVEX, Băile Govora, Romania (Vol. 2018, pp. 7- 9).

[8] Yamashita, T. and Hayes, P., 2008. Analysis of XPS spectra of Fe2+ and Fe3+ ions in oxide materials. Applied surface science, 254(8), pp.2441-2449.

[9] Sun, R.B., Xi, Z.G., Chao, F.H., Zhang, W., Zhang, H.S. and Yang, D.F., 2007. Decomposition of low-concentration gas- phase toluene using plasma-driven photocatalyst reactor. Atmospheric Environment, 41(32), pp.6853-6859.

[10] Yadav, A.A., Kang, S.W. and Hunge, Y.M., 2021. Photocatalytic degradation of Rhodamine B using graphitic carbon nitride photocatalyst. Journal ofMaterials Science: Materials in Electronics, 32(11), pp.15577-15585.

[11] Bie, C., Yu, H., Cheng, B., Ho, W., Fan, J. and Yu, J., 2021. Design, fabrication, and mechanism of nitrogen-doped graphene-based photocatalyst. Advanced Materials, 33(9), p.2003521.

[12] Rajaitha, P.M., Hajra, S., Sahu, M., Mistewicz, K., Toroń, B., Abolhassani, R., Panda, S., Mishra, Y.K. and Kim, H.J., 2022. Unraveling highly efficient nanomaterial photocatalyst for pollutant removal: a comprehensive review and future progress. Materials Today Chemistry, 23, p.100692.

[13] Wang, L., Cheng, B., Zhang, L. and Yu, J., 2021. In situ irradiated XPS investigation on S-scheme TiO2@ ZnIn2S4 photocatalyst for efficient photocatalytic CO2 reduction. Small, 17(41), p.2103447.

[14] Zhang, X., Chen, J., Jiang, S., Zhang, X., Bi, F., Yang, Y., Wang, Y. and Wang, Z., 2021. Enhanced photocatalytic degradation of gaseous toluene and liquidus tetracycline by anatase/rutile titanium dioxide with heterophase junction derived from materials of Institut Lavoisier-125 (Ti): Degradation pathway and mechanism studies. Journal of Colloid and Interface Science, 588, pp.122-137.

[15] Jin Huang (2023) XRD pattern offour catalysts

[16] Jin Huang (2023) Photocatalytic reaction loaded ≈ (RbLaNb2O6-xNx) nanosheets in C 1s; O 1s; N 1s; and Ce3d XPS narrow spectra.

[17] Jin Huang (2023) Photocatalytic reaction loaded ≈ (RbNdNb2O6-xNx) nanosheets in C 1s; O 1s; N 1s; and Ce3d XPS narrow spectra

[18] Jin Huang (2023) Photocatalytic reaction loaded ≈ (RbPrNb2O6-xNx) nanosheets in C 1s; O 1s; N 1s; and Ce3d XPS narrow spectra

[19] Jin Huang (2023) Photocatalytic reaction loaded ≈ (RbCeNb2O6-xNx) nanosheets in C1s; O1s; N1s; and Ce3d XPS narrow spectra

[20] Jin Huang (2023) The SEM images of the four catalysts (a= RbLaNb2O6-xNx; b= RbPrNb2O6-xNx; c = RbNdNb2O6-xNx; d=RbCeNb2O6-xNx

[21] Jin Huang (2023) Gas Chromatography of Four Catalysts

[22] Jin Huang (2023) The TEM image ofRbCeNbO6-xN